inorganics

MDPI

Article

Structural and Optical Properties of $BaWO_4$ Obtained by Fast Mechanochemical Treatment

Maria Gancheva [1,*], Reni Iordanova [1], Iovka Koseva [1], Iskra Piroeva [2] and Petar Ivanov [3]

[1] Institute of General and Inorganic Chemistry, Bulgarian Academy of Science, Acad. G. Bonchev str., bl.11, 1113 Sofia, Bulgaria; reni@svr.igic.bas.bg (R.I.); ikosseva@svr.igic.bas.bg (I.K.)
[2] Institute of Physical Chemistry, "Acad. Rostislaw Kaischew", Bulgarian Academy of Sciences, Acad. G. Bonchev str., bl. 11, 1113 Sofia, Bulgaria; ipiroeva@ipc.bas.bg
[3] Institute of Optical Materials and Technologies, "Acad. Jordan Malinowski", Bulgarian Academy of Sciences, Acad. G. Bonchev str, bl. 109, 1113 Sofia, Bulgaria; petar@iomt.bas.bg
* Correspondence: m.gancheva@svr.igic.bas.bg; Tel.: +359-2-979-35-88

Abstract: This work investigated the optical characteristics of $BaWO_4$ nanoparticles that were produced through direct mechanochemical synthesis at varying speeds and times. This research expands upon our previous study. We demonstrated that the mechanochemical activation of the precursor of $BaCO_3$ and WO_3, at elevated milling speeds (850 rpm), facilitates the formation of tetragonal $BaWO_4$ in a reduced reaction time. The final products were characterized by scanning electron microscopy (SEM), as well as Raman, infrared (IR), UV-Vis diffuse reflectance, and photoluminescence spectroscopies. The crystallite sizes and particles shapes were determined by X-ray diffraction and SEM analysis. Round particles with a size below 50 nm formed under different milling conditions. The Raman spectra of the synthesized samples confirmed the presence of a scheelite-type structure with the typical six distinct vibrational peaks. The symmetry of the structural WO_4 groups was determined by IR spectroscopy. The absorption spectra of both samples exhibited intensive peaks at 210 nm, and the calculated optical band gaps of $BaWO_4$ were 5.10 eV (3 h/500 rpm) and 5.24 eV (1 h/850 rpm). A strong (400 nm) and weak (465 nm) emission were observed for the $BaWO_4$ that was obtained at a higher milling speed, while wider emission at 410 nm was visible for the $BaWO_4$ that was prepared at a lower milling speed. The CIE coordinates of the mechanochemically synthesized $BaWO_4$ were located within the blue area, exhibiting various positions.

Keywords: ball milling; $BaWO_4$nanoparticles; Raman; IR; UV-Vis; blue emission

check for updates

Academic Editor: Hans Riesen

Received: 11 April 2025
Revised: 2 May 2025
Accepted: 7 May 2025
Published: 18 May 2025

Citation: Gancheva, M.; Iordanova, R.; Koseva, I.; Piroeva, I.; Ivanov, P. Structural and Optical Properties of $BaWO_4$ Obtained by Fast Mechanochemical Treatment. *Inorganics* **2025**, *13*, 172. https://doi.org/10.3390/inorganics13050172

Copyright: © 2025 by the authors. Licensee MDPI, Basel, Switzerland. This article is an open access article distributed under the terms and conditions of the Creative Commons Attribution (CC BY) license (https://creativecommons.org/licenses/by/4.0/).

1. Introduction

Alkaline–earth metal tungstates with the general formula AWO_4 (A =Ca, Ba, Sr) have good thermal and chemical stability and have been studied across various technical and scientific areas. Barium tungstate ($BaWO_4$) relates to this group, possesses a scheelite-type tetragonal structure, and has practical applications in several fields, such as dielectric materials [1–4], sensors [5], stimulated Raman scattering active media [6,7], optical materials [1,8–23], host matrices for doping by lanthanide-activated ions [24–31], and catalysts [17,19–21,32–34].

In the crystal lattice of $BaWO_4$, barium (Ba) atoms are surrounded by eight oxygen (O) atoms, while tungsten (W) atoms are coordinated with four oxygen atoms. This arrangement results in the formation of [BaO_8] deltahedral and [WO_4] tetrahedral groups [35]. It is well known that the properties and applications of nanomaterials depend on their composition,

structural units, crystallite size, and particle morphology and the method of synthesis. In general, the excitation and emission of MWO_4 compounds mainly arise from charge-transfer transitions within the $[WO_4]^{2-}$ groups [11,16,20,21,23]. Regarding optical applications, distortion into $[WO_4]$ groups and the formation of defects play important roles and can modify photoluminescent behavior [1,8,22,31]. According to the existing literature, the emission of $BaWO_4$ is observed in both regions from 390 to 460 nm and above 500 nm. This emission may comprise either a single or multiple peaks [1,8–23]. The blue emission band up to 425 nm is mainly attributed to the charge-transfer transitions within $[WO_4]^{2-}$ [10,11,15,21]. In addition to the blue emission in the range of 390–420 nm, four narrow peaks above 500 nm in $BaWO_4$ were reported. The authors explained the higher number of emission peaks with the formation of defects in the structure [16]. D. Sivaganesh et al. noted that the emission at 430 nm arises from two contributing factors: the distortion of the WO_4 tetrahedron and the presence of surface defects in $BaWO_4$ [22]. The emission at 460 and 485 nm is due to oxygen vacancies, caused by distorted WO_4 groups [8]. The green emission of $BaWO_4$ at 520 nm results from the formation of both barium and complex oxygen vacancies (neutral, and singly and doubly ionized oxygen vacations) during the preparation [17]. An emission at a higher wavelength of 540–550 nm occurred due to structural defects in the crystal phase [9,12,13,27]. A broad emission at 600 nm was observed for $BaWO_4$, originating from the defect centers associated with oxygen in the structure [18].

Some authors reported that a wider emission profile covering the full blue or green range is typical for multi-phonon and multi-level processes. These levels correspond to the various types of defects that are directly associated with the degree of structural order and disorder within the crystal structure [12,15,18,20]. The above-mentioned data indicated that the green emission of $BaWO_4$ is predominant, and it is observed when the excitation wavelength is higher (350 and 488 nm) [12,13,17,19,21]. There are sparse data about the blue emission of $BaWO_4$ only [11,23]. The appearance of the blue or green emission of $BaWO_4$ depends on the preparation method. The presence of different types of defects in the crystal structure of this phase has been determined by photoluminescence investigations [13,16,17,19–21].

$BaWO_4$ has been produced through various physico-chemical techniques, such as the combustion technique [1], the precipitation method [12,17,20,22,29], the Czochralski technique [10], microwave-assisted hydrothermal synthesis [12,13,21,24,25], microwave irradiation [15], the polymer micelle-assisted method [8,9], the sucrose-templated method [18], solid-state reaction [26,32], and mechanochemical synthesis [2,3,27,36]. For example, $BaWO_4$ with microwave dielectric properties was synthesized by mechanochemical activation of a mixture containing $BaCO_3$, WO_3, and H_2O, followed by thermal treatment at high temperatures [2,3]. R. C. Lima et al. investigated the photoluminescent properties of pure $BaWO_4$ that was obtained by the polymeric precursor method and subjected to mechanochemical activation for 4, 8, and 16 h [9]. They established that ball milling causes an emission peak at 590 nm, which is attributed to the structural disorder in the material. A mechanochemical reaction involving H_2WO_4, $BaCO_3$, Eu_2O_3, and C_2H_5OH was applied to prepare materials with LED applications [27]. In the literature, there are no data on the mechanochemical synthesis and optical properties of $BaWO_4$ that is doped with other rare earth active ions such as Dy^{3+}. As a first step, it is necessary to know the intensity and position of the emission peak of the host matrix, i.e., $BaWO_4$. Therefore, the ball milling processing of Dy^{3+}-doped $BaWO_4$ can be a suitable approach for determining the Dy^{3+} concentration and obtaining materials that will emit a white color.

In our earlier research, we successfully synthesized $BaWO_4$ at room temperature through mechanochemical processing at a speed of 500 rpm for 3 h [36].On the other hand, we show that mechanochemical treatment at different milling speeds is a rapid and productive method for the preparation of metal inorganic phases with a scheelite-type structure, which produces a strong blue emission at room temperature [37–39]. In this manner, we include new data on the fast preparation of materials for optical applications. Many research teams have used ball milling techniques for the synthesis of various functional materials. This process was performed using milling tools made of different materials (stainless steel, WC, and agate) at different processing times. It is well known that the milling parameters (speed, time, ball-to-powder mass ratio, and media) can be used to modify the properties of the final products. In general, a high ball-to-powder mass ratio and longer milling time at a higher speed can introduce a higher level of contamination in the treated sample [40]. Using a higher milling speed can effectively shorten the synthesis time and decrease the energy consumption compared to solution-based methods or classical solid-state reactions. The advantages of this approach are that the use of voluminous solutions and complicated operations, as well as the sintering of the final product, can be avoided. Therefore, the aim of this work was to investigate the phase formation of $BaWO_4$ at a milling speed of 850 rpm and carry out a comparative analysis of the structural, morphological, and optical properties of $BaWO_4$ obtained using milling speeds of 500 and 850 rpm.

2. Results

2.1. Phase Formation of $BaWO_4$ with an Applied Milling Speed of 850 rpm

2.1.1. X-Ray Diffraction Analysis

Our earlier investigations have shown that a higher milling speed is an important factor for the faster preparation of inorganic mixture materials with a scheelite-type structure [29–31]. This work added data on the phase formation of $BaWO_4$ at a milling speed of 850 rpm. The phase composition at each stage of the ball milling process was studied by X-ray diffraction analysis. The XRD patterns of the initial mixture exhibit the principal peaks of monoclinic WO_3 (PDF-01-072-0677) and hexagonal $BaCO_3$ (PDF-00-005-0378) (Figure 1). Ball milling treatment for 30 min led to the disappearance of the diffraction lines of the starting reagents. A set of new diffraction peaks of 2θ were observed at 17.50, 26.50, 28.05, 31.85, 43.0, 45.9, 48.70, 53.50, 54.40, 67.70, and 69.20°. They correspond to the (101), (112), (004), (200), (204), (132), (224) (208), (109), and (316) planes, which were indexed to the tetragonal scheelite-type structure of $BaWO_4$ (PDF-01-072-0746). The result is a good indication that a higher mechanical energy accelerates the chemical reaction for a short time. No other peaks were observed, which showed the existence of a single phase. Additional mechanochemical activation for up to 1 h did not lead to a significant change in the XRD pattern, which is an indication of the structural stability of this phase (Figure 1). The diffraction pattern exhibits wider diffraction lines, which are typical for the formation of a crystal phase in the nanosize range. The average crystallite size, D, was calculated from the strongest diffraction peak at 26.50° using the Scherrer formula, and it is 30 nm (±1 nm). A higher milling speed led to a short reaction time and produced a crystal phase with a larger crystallite size than the $BaWO_4$ that was obtained after 3 h of milling time at 500 rpm [36].

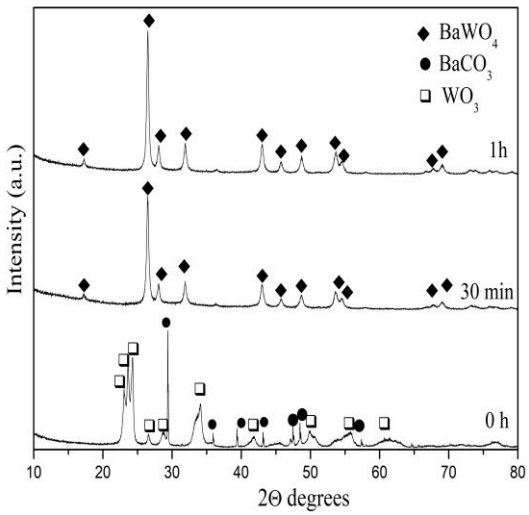


Figure 1. XRD pattern of the initial mixture, mechanochemically activated at 850 rpm.

2.1.2. Vibrational Spectroscopy

Using Raman and IR spectroscopies, we confirmed the formation of $BaWO_4$ under different ball milling conditions (500 and 850 rpm). We conducted a comparative analysis of the Raman and IR spectra of both $BaWO_4$ samples to obtain structural information regarding the symmetry of the WO_4 groups. The group theory shows that the scheelite structures have 26 distinct vibration modes with a zero wavevector (k = 0), as indicated by the following equation: Γ = (Raman + Infrared) = $3A_g + 5A_u + 5B_g + 3B_u + 5E_g + 5E_u$ [9,11,32,33]. For the Raman- and IR-active modes, the vibrations are reduced to $\Gamma = 3A_g + 4A_u + 5B_g + 5E_g + 4E_u$, where $3A_g + 4A_u$ and $5E_g$ belong to the Raman-active modes, while $4A_u$ and $4E_u$ are IR-active ones. The Raman spectra are registered from 130 to 1000 nm and contain well-defined bands related to the scheelite-type structure of both $BaWO_4$ phases, obtained using various milling speeds and times (Figure 2A). Raman bands at 925, 830, 795, 346, 334, and 185 cm^{-1} were detected in both spectra. The most intensive bands were registered at 925 and 334 cm^{-1}. The assignment of the Raman peaks is as follows: the band at 925 cm^{-1} is due to the ν_1 (A_g) symmetric stretching of WO_4 groups. The low intensive peaks at 830 and 795 cm^{-1} are the results of ν_3 asymmetric stretching (B_g and E_g) of the same units. The low-frequency lines at 334 cm^{-1} and the shoulder at 346 cm^{-1} arise from the activation of ν_2 (A_g) and ν_4 (B_g) vibrations, respectively. The free rotation mode ($\nu_{f.r.}$) was detected at 185 cm^{-1}. The observed Raman bands are in great agreement with literature data [12,13,16,17,40–42].

Infrared spectroscopy was employed to examine the degree of symmetry of the main structural groups in the crystal or amorphous phases (Figure 2B). The IR spectra of both samples show the typical bands of vibration of WO_4 units, based on the $BaWO_4$ structure [12,17,20,43]. The strong absorption band at 825 cm^{-1} was attributed to the ν_3 antisymmetric stretching vibration of WO_4 units of the sample obtained at a lower milling speed (500 rpm) [12,16,17,20]. The band position was shifted at lower wavenumbers up to 815 cm^{-1} in the IR spectrum of the $BaWO_4$ that was prepared at a high milling speed (850 rpm). The shoulder at 850 cm^{-1} was visible in the same IR spectrum. The variation in the band position and presence of a shoulder, which is typical of ν_3 vibration, are due to the deformation of the WO_4 that was induced by the higher milling speed. L. S. Cavalcante et al. also noted that the small deviation in the position of the ν_3 band and appearance of the shoulder are linked to distortions within the tetrahedral groups, caused by microwave radiation [12,13]. The weak band at a higher frequency of 925 cm^{-1} arises from the activation of the ν_1 mode associated with the WO_4 units. [43]. The difference in both IR spectra is evidence that WO_4 symmetry strongly depends on the applied milling speed. It is likely

that the development of deformed structural units is a result of the short reaction time associated with the increased milling speed.

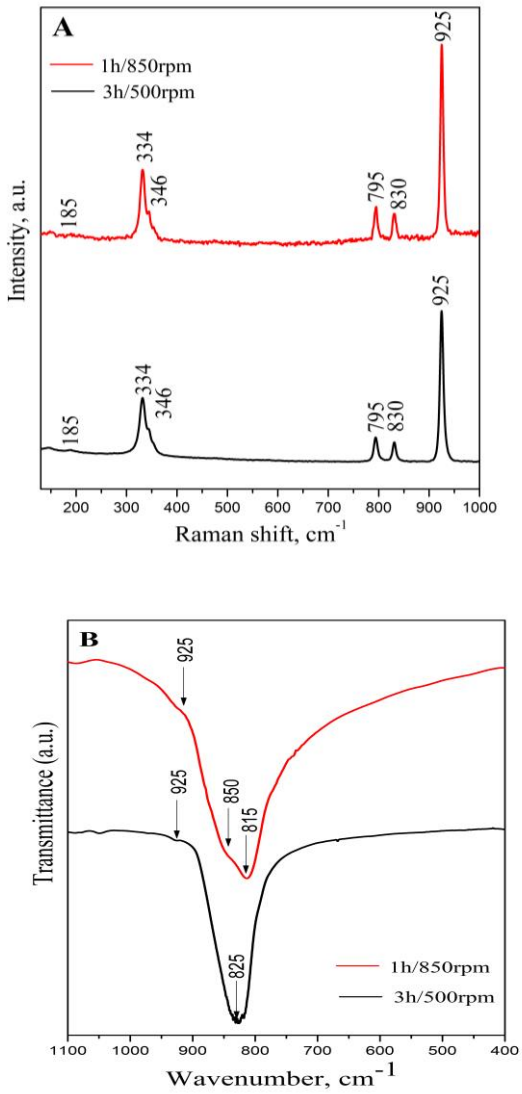


Figure 2. (**A**) Raman spectra of $BaWO_4$ samples obtained at various milling speeds and milling time. (**B**) IR spectra of the $BaWO_4$ samples obtained at various milling speeds and milling time.

2.1.3. SEM Analysis

The SEM images show the particle evolution of $BaWO_4$ depending on the milling speed. Figure 3A,B presents the morphology at different magnifications of the sample that was obtained after a 3 h milling time using 500 rpm. As can be seen from the figure, most of the particles are round with flat surfaces. Some of them have edges that form the hexagonal forms of the individual grains. Aggregation of the different types of particles was observed. The particle size histogram shows that the average size of a grain is 40.30 nm, and the particles possess a size range from 32 to 47 nm (Figure 3D). A similar tendency for the formation of particles with different shapes was detected in the SEM images of the $BaWO_4$ that was obtained after a 1 h milling time at 850 rpm (Figure 4A,B). The particles have a spherical shape and a flat surface without a clearly defined habit. The number of hexagonal particles is more negligible than in the sample obtained by a longer milling time at 500 rpm. The SEM micrographs exhibit agglomerated nanoparticles with non-uniform sizes and imperfect forms. The resultant particle size distribution histogram is depicted in Figure 4D. In this case, the average particle size is higher (48.80 nm), and

particles are in the size range of 37–57 nm. The EDS element mapping of both samples confirmed the presence of W, Ba, and O elements, whose distribution is homogenous (Figures 3C and 4C).

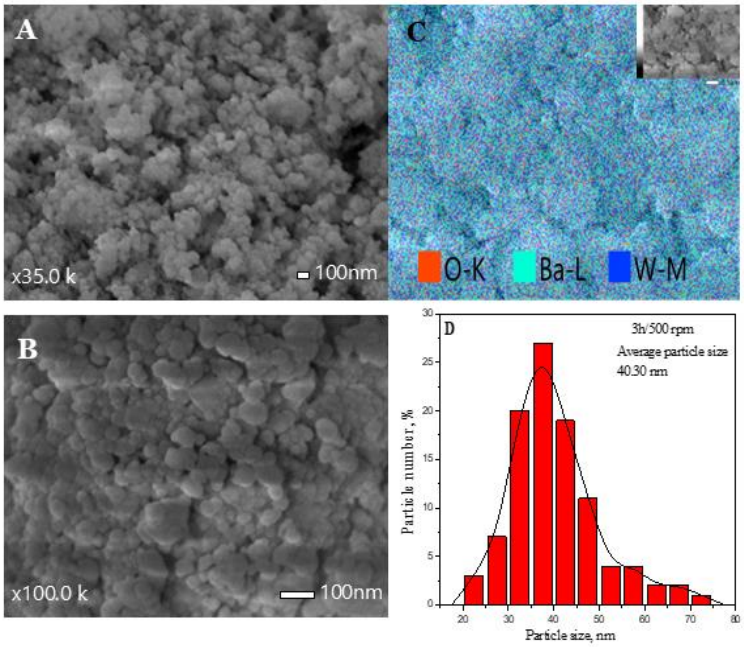


Figure 3. SEM images (**A**,**B**), EDS mapping (**C**), and particle size distribution (**D**) of $BaWO_4$ sample obtained after 3 h milling time using milling speed of 500 rpm.

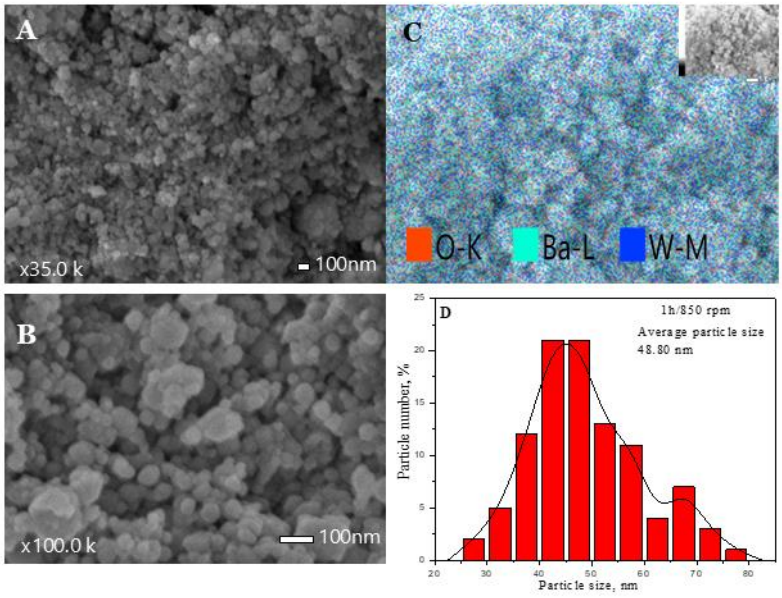


Figure 4. SEM images (**A**,**B**), EDS mapping (**C**), and particle size distribution (**D**) of $BaWO_4$ sample obtained after 1 h milling time using milling speed of 850 rpm.

2.2. Optical Properties

2.2.1. UV–Vis Diffuse Reflectance Spectroscopy

The UV-Vis and photoluminescence spectroscopies were applied to study the optical properties of the $BaWO_4$ samples. Figure 5 illustrates the UV-Vis spectra of $BaWO_4$ powders obtained at different mechanochemical activations. The absorption spectator contains a strong peak at 210 nm and weak ones at 260 and 330 nm. The intensity of the main

peak is slightly higher when the sample was synthesized at an increased milling speed, probably due to the higher crystallite size. The band observed at 210 nm is linked to charge-transfer transitions occurring within the $[WO_4]^{2-}$ groups, which is typical for scheelite-type inorganic phases [1,18,19,38]. The peak at 330 nm is associated with the formation of the excitonic state on Ba^{2+} in the crystal structure [38,44]. The optical band gap values of both samples were estimated using the Tauc equation, $h\nu\alpha = A(h\nu - Eg)^n$, where α is the absorbance, h is the Planck constant, ν is the frequency, and n is a constant associated with the different types of electronic transitions (allowed direct, allowed indirect, forbidden direct, and forbidden indirect) [45]. In this case, for the determination of the optical band gap, the value of n is 0.5 in accordance with the literature data [46]. The calculated values of the optical band gaps of BaWO4 are 5.10 (3 h/500 rpm) and 5.24 eV (1 h/850 rpm), respectively (inset of Figure 5). The increase in milling time up to 3 h led to a reduction in the Eg of the obtained phase. We observed a tendency for a decreasing optical band gap after longer reaction times for the mechanochemical synthesis of other crystal phases with scheelite-type structures [30,31]. Comparable behavior was also reported for $BaWO_4$ prepared by the microwave hydrothermal route at 140°C for different durations and for $BaWO_4$ obtained by the polymeric precursor method, followed by ball milling for up to 16 h [14]. The determined values of the optical band gaps of the as-prepared samples are higher than those of $BaWO_4$ that was synthesized by combustion [1], coprecipitation [17,20], the microwave hydrothermal method [13], and solid-state reaction [32]. This fact can be attributed to the stronger ball milling conditions and shorter reaction time. It is reported that the optical band gap of $BaWO_4$ can be in the range from 3.84 to 5.76 eV, and it depends on the methods of synthesis [9,13,17,18,20–22].

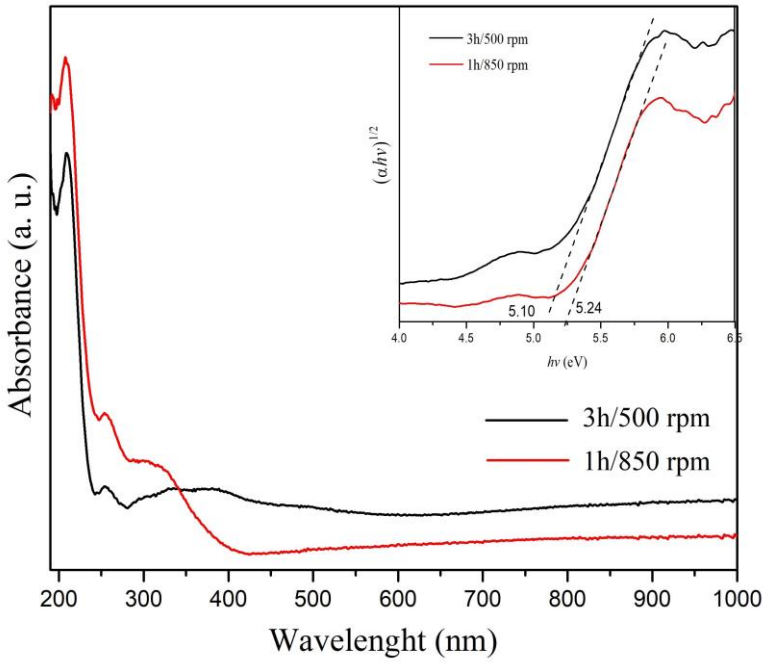


Figure 5. UV–vis absorbance spectra of $BaWO_4$ samples obtained at various milling speeds and milling times. Plot of $(\alpha h\nu)^{1/2}$ versus photon energy ($h\nu$) indicates presence in the inset.

2.2.2. Photoluminescence Emission Spectroscopy

Figure 6 shows the emission spectra of mechanochemically synthesized $BaWO_4$ at 500 and 850 rpm under an excitation wavelength of 250 nm. It can be seen that the emission behavior of the samples is different depending on the milling speeds. A narrow emission spectrum with a maximum at 400 and a weak peak at 465 nm was observed for $BaWO_4$ that was prepared using a 1 h milling time at 850 rpm. The peak at 400 nm is typical

for the transfer of oxygen to central tungstate in $[WO_4]^{2-}$ groups [10–12,15,21,23]. The appearance of the emission at 465 nm was due to oxygen vacations caused by the distorted WO_4 tetrahedral group because of the introduced higher milling energy. The formation of asymmetrical WO_4 in this sample was confirmed through IR analysis (Figure 2B). In the literature, there are data on the presence of oxygen vacations in the crystal phases, identified by PL analysis [47–49]. For example, Z. Li et al. reported that the blue-light component (450 nm) in the emission spectrum of $SrTiO_3$ can be attributed to oxygen deficiency within the structure [47]. A. K. Kunti et al. assigned the emission peak at 470 nm in TiO_2 to the presence of oxygen vacancies [48]. In this case, the spectral features of photoluminescence (PL) spectra serve as indirect evidence of the nature of defects in semiconductors. In our previous study, we demonstrated that a higher milling speed (850 rpm) led to the formation of Frenkel defects in $SrMoO_2$, as established by photoluminescence spectroscopy [39]. At a lower milling speed of 500 rpm, the emission becomes broader, and the peak shifts up to 410 nm. This peak loses its intensity and merges with the green emission from 450 to 550 nm as a tail. The absence of a distinct band in this range probably means that the formation of oxygen vacancies is reduced when using a lower milling speed. The changed position of the main peak is due to the prolonged reaction time and decreased crystallite size of the $BaWO_4$ [47]. The PL profiles of both samples are asymmetrical and typical for inorganic mixture oxides with a scheelite-type structure that are synthesized by direct mechanochemical treatment [37–39]. T. Thongtem et al. reported that $BaWO_4$ that was obtained by the sonochemical method displays an asymmetric emission line with a maximum peak at 418 nm [11]. On the other hand, a symmetrical PL profile with a peak at 410 nm was observed for $BaWO_4$ that was synthesized by the hydrothermal route [23]. Figure 6 further demonstrates the influence of the crystallite size and the symmetry of WO_4 groups on the photoluminescence (PL) intensity in both samples. $BaWO_4$ with a higher crystallite size and more distorted WO_4 units, exhibits a higher emission intensity compared to the sample with smaller crystallites and symmetrical WO_4 groups. In our previous study, we pointed out that a higher emission intensity will increase the crystallite size and formation of asymmetric structural units [30]. Additionally, the reduced intensity of the main emission peak can be attributed to the prolonged duration of the mechanochemical treatment. K.P. Shinde et al. observed that the strength of the emission line of ZnO significantly diminished as the duration of ball milling increased [50]. Based on IR and PL analyses, we conclude that a milling speed of 850 rpm promotes the formation of $BaWO_4$ with more asymmetric WO_4 groups, as evidenced by the splitting of the band associated with the ν_3 vibration and the presence of oxygen vacations, indicated by the emission peak at 465 nm.

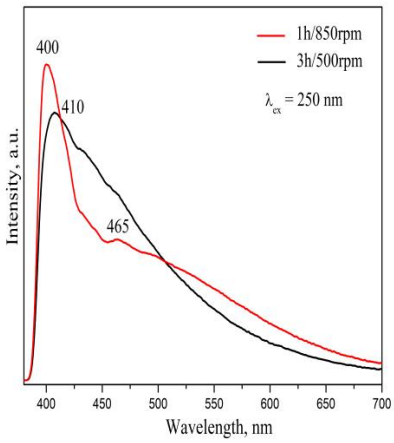


Figure 6. Photoluminescent emission spectra of $BaWO_4$ samples obtained at various milling speeds and milling times.

The CIE (International Commission on Illumination) chromaticity diagram of both $BaWO_4$ samples is presented in Figure 7. The chromaticity coordinates (x, y), calculated from the emission spectra, were found to be x = 0.246 and y = 0.270, and x = 0.208 and y = 0.208 for $BaWO_4$ obtained using higher and lower milling speeds, respectively. This result indicates a shift in emission color from deep blue to light blue as the milling speed decreases.

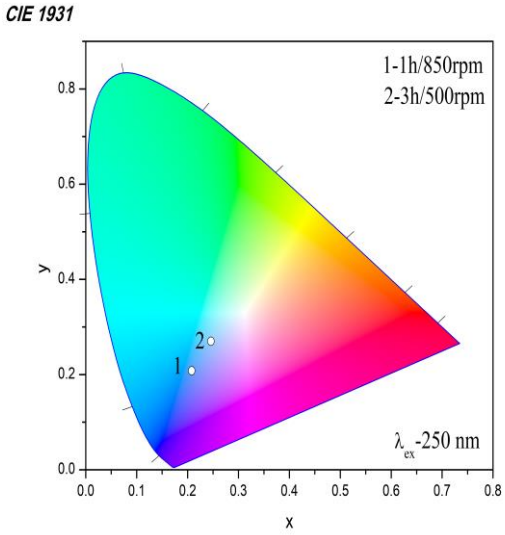


Figure 7. CIE diagram of $BaWO_4$ samples obtained at various milling speeds and milling times.

3. Discussion

The results obtained from the IR and PL spectroscopies for both samples indicate that the milling speed influences the symmetry of WO_4 units and the formation of oxygen vacations. A higher milling speed led to the formation of asymmetric WO_4, which was connected to the appearance of a shoulder at 850 cm^{-1} in the IR spectrum of the sample. The presence of the peak at 465 nm in the emission spectrum is attributed to the creation of oxygen defects as a result of the destroyed WO_4 groups. The above-mentioned facts led to variations in the emission profiles and changes in peak positions, intensities, and CIE coordinates. This research shows that the mechanochemical method is a fast route for obtaining optical materials. Also, this approach can be used to prepare lanthanide-activate ions dopped $BaWO_4$ phases for changing the color tun.

4. Materials and Methods

A mixture of $BaCO_3$ (Merck, KGaA, Amsterdam, The Netherlands, purity 99.9%) and WO_3 (Merck, KGaA, Amsterdam, The Netherlands, purity 99.9%) at a molar ratio of 1:1 was subjected to intense mechanical treatment in a planetary ball mill (Fritsch–Premium line–Pulversette No 7, Idar-Oberstein Germany). Both vials and balls were made of stainless steel, the milling rotation speed was 850 rpm, the milling duration was up to 1 h, and the ball-to-powder mass ratio was 10:1. The ball milling was carried out in an air atmosphere. To minimize the temperature, which rose during the milling, the process was carried out for periods of 15 min, with rest periods of 5 min [28–31].

The phase formation of the crystal phase was monitored by X-ray powder diffraction analysis (XRD) on a Bruker D8 Advance instrument (Karlsruhe, Germany) equipped with a copper tube (CuKα) and a position-sensitive LynxEye detector. The diffraction patterns were taken in the angular range of 10–80.00° 2θ with a step of 0.04° 2θ and counting time of 0.1 s for each individual strip of the detector (total 17.5 s/step). The morphology of the samples was studied using a field-emission scanning electron microscope, JEOL IT800SHL

(Tokyo, Japan), in both secondary and backscattered electron detectors, placed in-chamber and using an in-lens microscope column. The Raman spectra were recorded on a Via Qontor Raman Confocal Microscope (Renishaw plc, Wotton-under-Edge, England, UK) with a laser wavelength of 532 nm (Nd:YAG-Laser). The laser power on the sample was kept up to 1% of the nominal power, so no heating effects on the powder sample could be observed. The excitation light was focused and collected using a ×50 LWD objective lens. The infrared spectra were registered at room temperature in the range of 1100–400 cm^{-1} by a Nicolet-320 FTIR spectrometer (Madison, WI, USA). The sample was pressed into a thick pellet diluted with KBr. The spectral resolution was 2 nm for measurements. The diffuse reflectance spectra were recorded with a Thermo Evolution 300 UV-Vis Spectrophotometer (Madison, WI, USA) equipped with a Praying Mantis device. Spectralon was used as a standard material (100% reflectance) for background calibration. The photoluminescence emission spectra were measured on a Horiba Fluorolog 3-22 TCS spectrophotometer (Longjumeau, France) equipped with a 450 W Xenon Lamp as the excitation source. All spectra were recorded at an ambient temperature.

5. Conclusions

It was established that the milling speed significantly influences the reaction time, crystallite and particle size, and structural and optical properties of $BaWO_4$. A higher milling speed of 850 rpm led to faster synthesis, while a lower speed of 500 rpm prolonged the reaction time up to 3 h. The formation of single-phase $BaWO_4$ with a scheelite-type structure was confirmed by XRD and Raman analysis. Both samples exhibited similar particle morphologies, characterized by predominantly rounded grains with varying degrees of agglomeration. The IR spectroscopy revealed that a higher milling speed leads to the formation of WO_4 units with less symmetry, while the lower milling speed produces symmetrical WO_4 groups. The optical band gap of $BaWO_4$ decreases from 5.24 eV to 5.10 eV with the increase in reaction time at a lower milling speed. The presence of defects in $BaWO_4$ was analyzed through the measurement of photoluminescence (PL) spectra at room temperature. The $BaWO_4$ that was obtained using a higher milling speed showed strong (400 nm) and weak band (465 nm) emissions, which can be attributed to the larger crystallite size, deformed WO_4 units, and oxygen vacancy defects. A single emission peak at 410 nm was observed in the $BaWO_4$ that was obtained at a milling speed of 500 rpm, which was attributed to the lower crystallite size and symmetrical WO_4 groups. The as-prepared $BaWO_4$ samples possessed different chromaticity coordinates in the blue area in the CIE diagram. These results indicate that mechanochemical synthesis is highly important for the preparation of blue-emitting components for optical devices.

Author Contributions: Conceptualization, M.G.; methodology, M.G., R.I., and I.K.; SEM investigation I.P., software, I.K and P.I.; validation, M.G. and I.K.; formal analysis, M.G. and I.K.; investigation, M.G., R.I., and I.K.; data curation, I.K., writing—original draft preparation, M.G. and I.K.; writing—review and editing, R.I.; visualization, M.G. and I.K.; R.I. All authors have read and agreed to the published version of the manuscript.

Funding: This research received no external funding.

Institutional Review Board Statement: Not applicable.

Informed Consent Statement: Not applicable.

Data Availability Statement: The original contributions presented in this study are included in the article.

Acknowledgments: Research equipment from the distributed research infrastructure INFRAMAT (part of Bulgarian National roadmap for research infrastructures), supported by Bulgarian Ministry

of Education and Science under contract D01-322/30, November 2023, was used in this investigation. The Raman equipment and investigation were used within the framework of the "Center of excellence mechatronics and clean technologies", with financial support from the European regional development fund within the program "Research, Innovation and Digitalisation for Smart Transformation, 2021–2027".

Conflicts of Interest: The authors declare no conflicts of interest.

References

1. Vidya, S.; Solomon, S.; Thomas, J.K. Synthesis, Characterization, and Low Temperature Sintering of Nanostructured $BaWO_4$ for Optical and LTCC Applications. *Adv. Conden. Matter Phys.* **2013**, *1–2*, 409620–409631.
2. Cheng, L.; Liu, P.; Qu, S.X.; Zhang, H.W. Microwave dielectric properties of AWO_4 (A = Ca, Ba, Sr) ceramics synthesized via high energy ball milling method. *J. Alloys Compd.* **2013**, *581*, 553–557. [CrossRef]
3. Guia, L.; Yanga, H.; Zhao, Q.; Li, E. Synthesis of low temperature firing scheelite-type $BaWO_4$ microwave dielectric ceramics with high performances. *Ceram. Int.* **2018**, *46*, 1360–1365. [CrossRef]
4. Ren, Y.; Wang, J.; Guo, Y.; Li, D.; Li, J. Sintering behavior, lattice vibrational characteristics and dielectric properties of B-site ion substituted $BaWO_4$ ceramics for LTCC applications. *J. Alloys Compd.* **2025**, *1010*, 177261–177273. [CrossRef]
5. Hemmati, M.; Tafreshi, M.J.; Ehsani, M.H.; Alamdari, S. Highly sensitive and wide-range flexible sensor based on hybrid $BaWO_4$ @CS nanocomposite. *Ceram. Int.* **2022**, *48*, 26508–26518. [CrossRef]
6. Sulc, J.; Jelınkova, H.; Basiev, T.T.; Doroschenko, M.E.; Ivleva, L.I.; Osiko, V.V.; Zverev, P.G. Nd: $SrWO_4$ and Nd:$BaWO_4$ Raman lasers. *Opt. Mater.* **2007**, *30*, 195–197. [CrossRef]
7. Kinyaevskiy, I.O.; Koribut, A.V.; Seleznev, L.V.; Grudtsyn, Y.V. Stimulated Raman scattering of titanium-sapphire laser pulses with duration from 7 ps to 45ps in $BaWO_4$ crysral. *Opt. Spectrosc.* **2024**, *132*, 49–52.
8. Zhou, G.; Lu, M.; Xiu, Z.; Wang, S.; Zhang, H.; Zou, W. Polymer micelle-assisted fabrication of hollow $BaWO_4$ nanospheres. *J. Cryst. Growth* **2005**, *276*, 116–120. [CrossRef]
9. Lima, R.C.; Anicete-Santos, M.; Orhan, E.; Maurera, M.A.M.A.; Souza, A.G.; Pizani, P.S.; Leite, E.R.; Varela, J.A.; Longo, E. Photoluminescent property of mechanically milled $BaWO_4$ powder. *J. Lumin.* **2007**, *126*, 741–746. [CrossRef]
10. Tyagi, M.; Sabharwal, S.S.C. Luminescence properties of $BaWO_4$ single crystal. *J. Lumin.* **2008**, *128*, 1528–1532. [CrossRef]
11. Thongtema, T.; Phuruangrat, A.; Thongtem, S. Characterization of $MeWO_4$ (Me = Ba, Sr and Ca) nanocrystallines prepared by sonochemical method. *Appl. Surf. Sci.* **2008**, *254*, 7581–7585. [CrossRef]
12. Cavalcante, L.S.; Sczancoski, J.C.; Lima, L.F.; Espinosa, J.W.M.; Pizani, P.S.; Varela, J.A.; Longo, E. Synthesis, Characteri-zation, Anisotropic Growth and Photoluminescence of $BaWO_4$. *Cryst. Growth Des.* **2009**, *9*, 1002–1012. [CrossRef]
13. Cavalcante, L.S.; Sczancoski, J.C.; Espinosa, J.W.M.; Varela, J.A.; Pizani, P.S.; Longo, E. Photoluminescent behavior of $BaWO_4$ powders processed in microwave-hydrothermal. *J. Alloys Coumpd.* **2009**, *474*, 195–200. [CrossRef]
14. Yin, Y.; Gan, Z.; Sun, Y.; Zhou, B.; Zhang, X.; Zhang, D.; Gao, P. Controlled synthesis and photoluminescence properties of $BaXO_4$ (X = W, Mo) hierarchical nanostructures via a facile solution route. *Mater. Lett.* **2010**, *64*, 789–792. [CrossRef]
15. Shen, Y.; Li, W.; Li, T. Microwave-assisted synthesis of $BaWO_4$ nanoparticles and its photoluminescence properties. *Mater. Lett.* **2011**, *65*, 2956–2958. [CrossRef]
16. Lim, C.S. Solid-state metathetic synthesis of $BaMO_4$ (M = W, Mo) assisted by microwave irradiation. *J. Ceram. Proc. Res.* **2011**, *12*, 544–548.
17. Cavalcante, L.S.; Batista, F.M.C.; Almeida, M.A.P.; Rabelo, A.C.; Nogueira, I.C.; Batista, N.C.; Varela, J.A.; Santos, M.R.M.C.; Longo, E.; Li, M.S. Structural refinement, growth process, photoluminescence and photocatalytic properties of (Ba1-xPr2x/3)WO_4 crystals synthesized by the coprecipitation method. *RSC Adv.* **2012**, *2*, 6438–6454. [CrossRef]
18. Zawawi, S.M.M.; Yahya, R.; Hassan, A.; Mahmud, H.N.M.E.; Daud, M.N. Structural and optical characterization of metal tungstates (MWO_4; M=Ni, Ba, Bi) synthesized by a sucrose-templated method. *Chem. Cent. J.* **2013**, *7*, 80–90. [CrossRef]
19. Sadiq, M.M.J.; Nesaraj, A.S. Soft chemical synthesis and characterization of $BaWO_4$ nanoparticles for photocatalytic removal of Rhodamine B present in water sample. *J. Nanostruct. Chem.* **2015**, *5*, 45–54. [CrossRef]
20. Shivakumara, C.; Saraf, R.; Behera, S.; Dhananjaya, N.; Nagabhushana, H. Scheelite-type MWO_4 (M = Ca, Sr, and Ba) nanophosphors: Facile synthesis, structural characterization, photoluminescence, and photocatalytic properties. *Mater. Res. Bull.* **2015**, *61*, 422–432. [CrossRef]
21. Mesquita, F.A.; Feitosa, C.A.C.; Balzer, R.; Probst, L.F.D.; Batalha, D.C.; Rosmaninho, M.G.; Fajardo, H.V.; Bernardi, M.I.B. Preparation, characterization and catalytic application of Barium molybdate ($BaMoO_4$) and Barium tungstate ($BaWO_4$) in the gas-phase oxidation of toluene. *Ceram. Int.* **2017**, *43*, 4462–4469.
22. Sivaganesh, D.; Saravanakumar, S.; Ali, K.S.S.; Alshehri, A.M. Effect of preparation techniques on $BaWO_4$: Structural, morphological, optical and electron density distribution analysis. *J. Mater. Sci. Mater. Electron.* **2021**, *32*, 1466–1475. [CrossRef]

23. Kowalkinska, M.; Głuchowski, P.; Swebocki, T.; Ossowski, T.; Ostrowski, A.; Bednarski, W.; Karczewski, J.; Zielinska-Jurek, A. Scheelite-Type Wide-Band gap ABO_4 Compounds (A = Ca, Sr, and Ba; B = Mo and W) as Potential Photocatalysts for Water Treatment. *J. Phys. Chem. C* **2021**, *125*, 25497–25513. [CrossRef]
24. Liao, J.; Qiu, B.; Wen, H.; You, W.; Xiao, Y. Synthesis and optimum luminescence of monodispersed spheres for $BaWO_4$-based green phosphors with doping of Tb^{3+}. *J. Lumin.* **2010**, *130*, 762–766. [CrossRef]
25. Jia, G.; Dong, D.; Song, C.; Li, L.; Huang, C.; Zhang, C. Hydrothermal synthesis and luminescence properties of monodisperse $BaWO_4$: Eu^3 submicrospheres. *Mater. Lett.* **2014**, *129*, 251–254. [CrossRef]
26. Bouzidi, C.; Ferhi, M.; Elhouichet, H.; Ferid, M. Spectroscopic properties of rare-earth (Eu^3, Sm^3) doped $BaWO_4$ powders. *J. Lumin.* **2015**, *161*, 448–455. [CrossRef]
27. Jena, P.; Gupta, S.K.; Verma, N.K.; Singh, A.K.; Kadam, R.M. Energy transfer dynamics and time resolved photolumines-cence in $BaWO_4$: Eu^{3+} nanophosphors synthesized by mechanical activation. *New J. Chem.* **2017**, *41*, 8947–8958. [CrossRef]
28. Carvalho, I.P.; Sousa, R.B.; Matos, J.M.E.; Moura, J.V.B.; Freire, P.T.C.; Pinheiro, G.S.; Luz-Lima, C. Low-temperature induced phase transitions in $BaWO_4$: Er3 + microcrystas: A Raman scattering study. *J. Mol. Struct.* **2020**, *1204*, 127497–127498. [CrossRef]
29. Jung, J.; Kim, J.; Shim, Y.S.; Hwang, D.; Son, C.S. Structure and Photoluminescence Properties of Rare-Earth (Dy^{3+}, Tb^{3+}, Sm^{3+})-Doped $BaWO_4$ Phosphors Synthesized via Co-Precipitation for Anti-Counterfeiting. *Materials* **2020**, *13*, 4165–4177. [CrossRef]
30. Gopal, R.; Manam, J. The photoluminescence and Judd-Ofelt investigations of UV, near-UV and blue excited highly pure red emitting $BaWO_4$: Eu^{3+} phosphor for solid state lighting. *Ceram. Int.* **2023**, *49*, 28118–28129. [CrossRef]
31. Paikray, X.S.; Ray, S.K.; Nayak, P.; Sahoo, A.K.; Prusty, S.N.; Dash, S.; Nanda, S.S. Comparative analysis of Sm^{3+}-doped $BaWO_4$ and $CaWO_4$ phosphors: Properties and application in latent fingerprints and anti-counterfeiting. *J. Alloys Compd.* **2025**, *1010*, 177666–177676. [CrossRef]
32. Shana, Z.; Wang, Y.; Ding, H.; Huang, F. Structure-dependent photocatalytic activities of MWO_4 (M = Ca, Sr, Ba). *J. Mol. Catal. A Chem.* **2009**, *302*, 54–58. [CrossRef]
33. Sridhar, C.; Seo, Y.S.; Rabani, I.; Turpu, G.R.; Tigga, S.; Padmaja, G. Electrochemical, Photocatalytic and Photolumines-cence properties of $BaWO_4$ and rGO-$BaWO_4$ nano-composites: A Comparative study. *Curr. Appl. Phys.* **2024**, *58*, 79–90. [CrossRef]
34. Jafar, M.; Kumar, A.; Gupta, V.G.; Tyagi, A.K.; Bhattacharyya, K. Scheelite Catalysts for Thermal Mineralization of Toluene: A Mechanistic Overview. *ACS Omega* **2025**, *10*, 13080–13104. [CrossRef]
35. Sleight, A.W. Accurate Cell Dimensions for ABO_4 Molybdates and Tungstates. *Acta Cryst. B* **1972**, *28*, 2899–2902. [CrossRef]
36. Gancheva, M.; Iordanova, R.; Avdeev, G.; Ivanov, P. Direct mechanochemical synthesis and optical properties of $BaWO_4$ nanoparticles. *Bulg. Chem. Commun.* **2022**, *54*, 41–46.
37. Gancheva, M.; Iordanova, R.; Koseva, I.; Avdeev, G.; Burdina, G.; Ivanov, P. Synthesis and Luminescent Properties of Barium Molybdate Nanoparticles. *Materials* **2023**, *16*, 7025–7706. [CrossRef]
38. Iordanova, R.; Gancheva, M.; Koseva, I.; Tzvetkov, P.; Ivanov, P. The Influence of High-Energy Milling on the Phase Formation, Structural, and Photoluminescent Properties of $CaWO_4$ Nanoparticles. *Materials* **2024**, *17*, 3724–3738. [CrossRef]
39. Gancheva, M.; Iordanova, R.; Avdeev, G.; Piroeva, I.; Ivanov, P. Direct mechanochemical synthesis of $SrMoO_4$: Structural and luminescence properties. *RSC Mechanochem.* **2025**, *2*, 459–467. [CrossRef]
40. Jablan, Z.J.; Marguí, E.; Posavec, L.; Klaric, D.; Cincic, D.; Galic, N.; Jug, M. Product contamination during mechanochemical synthesis of praziquantel co-crystal, polymeric dispersion and cyclodextrin complex. *J. Pharm. Biomed. Anal.* **2024**, *238*, 115855–115865. [CrossRef]
41. Porto, S.P.S.; Scott, J.F. Raman Spectra of CaWO, $SrWO_4$, $CaMoO_4$, and $SrMoO_4$. *Phys. Rev.* **1967**, *157*, 716–719. [CrossRef]
42. Suda, J.; Kusama, A.; Sato, T. The First-Order Raman Spectra and Lattice Dynamics for sintered body-centered tetragonal $BaWO_4$ Crystallinite. *J. Spectrosc. Soc. Jpn.* **2001**, *50*, 65–70. [CrossRef]
43. Miller, P.J.; Khanna, R.K.; Lippincott, E.R. Studies of coupled molybdate and tungstate vibrations. *J. Phys. Chem. Solids* **1973**, *34*, 533–540. [CrossRef]
44. Marquesa, A.P.A.J.; Meloa, D.M.A.; Longo, E.; Paskocimasa, C.A.; Pizanic, P.S.; Leite, E.R. Photoluminescence properties of $BaMoO_4$ amorphous thin films. *J. Solid State Chem.* **2005**, *178*, 2346–2353. [CrossRef]
45. Tauc, J. Absorption edge and internal electric fields in amorphous semiconductors. *Mater. Res. Bull.* **1970**, *5*, 721–729. [CrossRef]
46. Huang, Y.; Guo, Z.; Liu, H.; Zhang, S.; Wang, P.; Lu, Y.; Tong, Y. Heterojunction Architecture of N-Doped WO3 Nanobundles with Ce_2S_3 Nanodots Hybridized on a Carbon Textile Enables a Highly Efficient Flexible Photocatalyst. *Adv. Funct. Mater.* **2019**, *29*, 1903490–1903499. [CrossRef]
47. Li, Z.; Sun, H.; Xie, Z.; Zhao, Y.; Lu, M. Modulation of the photoluminescence of $SrTiO_3$(001) by means of fluorhydric acid etching combined with Ar+ ion bombardment. *Nanotechnology* **2007**, *18*, 165703–165708. [CrossRef]
48. Kunti, A.K.; Sekhar, K.C.; Pereira, M.; Gomes, M.J.M.; Sharma, S.K. Oxygen partial pressure induced effects on the micro-structure and the luminescence properties of pulsed laser deposited TiO2 thin films. *AIP Adv.* **2017**, *7*, 015021–015030. [CrossRef]

49. Gupta, S.K.; Sudarshan, K.; Srivastava, A.P.; Kadam, R.M. Visible light emission from bulk and nano $SrWO_4$: Possible role of defects in photoluminescence. *J. Lumin.* **2017**, *192*, 1220–1226. [CrossRef]
50. Shinde, K.P.; Pawar, R.C.; Sinha, B.B.; Kim, H.S.; Oh, S.S.; Chung, K.C. Study of effect of planetary ball milling on ZnO na-nopowder synthesized by co-precipitation. *J. Alloys Compnd.* **2014**, *617*, 404. [CrossRef]

Disclaimer/Publisher's Note: The statements, opinions and data contained in all publications are solely those of the individual author(s) and contributor(s) and not of MDPI and/or the editor(s). MDPI and/or the editor(s) disclaim responsibility for any injury to people or property resulting from any ideas, methods, instructions or products referred to in the content.